TRIM24 mediated YBX1 ubiquitination inhibits TMBIM6 m5C to block M2 polarization in nasopharyngeal carcinoma

Yi Li
First Affiliated Hospital of University of South China
Zhongyi Li
First Affiliated Hospital of University of South China
Junyan He
First Affiliated Hospital of University of South China
Chuangjie Cao
First Affiliated Hospital of University of South China
Aitao Nai
First Affiliated Hospital of University of South China
Yang Li
University of South China
Dong Yang
yangdong4168@163.com

First Affiliated Hospital of University of South China

Article

Keywords: Nasopharyngeal carcinoma, Tumor-associated macrophages, TRIM24, YBX1, TMBIM6

Posted Date: May 5th, 2026

DOI: https://doi.org/10.21203/rs.3.rs-9314803/v1

Additional Declarations: No competing interests reported.

Abstract

The immunosuppressive tumor microenvironment in nasopharyngeal carcinoma (NPC) is shaped by M2-polarized tumor-associated macrophages. While Transmembrane Bax Inhibitor Motif-containing 6 (TMBIM6) promotes tumor cell survival, its role in immune modulation is unknown. Here, we investigated a novel regulatory axis involving TRIM24, YBX1, and TMBIM6 in controlling macrophage polarization. Expression was analyzed in NPC samples and polarized macrophages, with gain- and loss-of-function studies performed in vitro. Mechanisms were dissected using co-immunoprecipitation, ubiquitination assays, MeRIP-qPCR, RNA stability, and dual-luciferase reporter assays. The Ca^{2+}/CaM/CaMKII pathway was examined with inhibitor KN93, and therapeutic potential was tested in a xenograft model combining macrophage targeting with anti-PD-L1 therapy. TMBIM6 was overexpressed in NPC tissues and specifically enriched in M2 macrophages. Knockdown of TMBIM6 in macrophages inhibited M2 polarization, suppressed their pro-tumor functions, and activated the Ca^{2+}/CaM/CaMKII pathway. Mechanistically, the RNA-binding protein YBX1 stabilized TMBIM6 mRNA via m5C modification, enhancing its expression. The E3 ubiquitin ligase TRIM24 targeted YBX1 for proteasomal degradation, acting as an upstream negative regulator. In vivo, conditioned medium from TMBIM6-knockdown macrophages significantly suppressed tumor growth, an effect synergistically enhanced by PD-L1 inhibitor combination. This study identifies a novel TRIM24/YBX1/TMBIM6/Ca^{2+} signaling axis that critically regulates M2 macrophage polarization in NPC. Targeting this pathway can reprogram the immunosuppressive tumor microenvironment and exhibits synergistic anti-tumor activity with immune checkpoint blockade, presenting a promising therapeutic strategy for NPC.

Introduction

Nasopharyngeal carcinoma (NPC) is associated with Epstein-Barr virus and shows a distinct geographical distribution, with the highest incidence in southern China [1, 2]. Despite improved local control with intensity-modulated radiotherapy, challenges remain in locally advanced patients, including radiotherapy resistance, distant metastasis, and limited response to immune checkpoint inhibitors [3, 4, 5, 6]. The immunosuppressive tumor microenvironment (TME) is a key contributor to treatment failure [7, 8, 9].

Within the TME, tumor-associated macrophages (TAMs) are abundant and plastic. They can polarize into anti-tumor M1 or pro-tumor M2 phenotypes [10, 11]. M2 TAM infiltration in NPC correlates with advanced stage, metastasis, and poor prognosis [6, 11, 12]. M2 TAMs promote tumor growth and immune escape by secreting immunosuppressive factors, inhibiting cytotoxic T cells, and enhancing angiogenesis and invasion [12, 13]. Thus, understanding M2 polarization mechanisms is vital for immunotherapy development.

Transmembrane Bax Inhibitor Motif-containing 6 (TMBIM6), an ER protein, regulates calcium homeostasis and inhibits apoptosis [13, 14]. TMBIM6 is upregulated in NPC and promotes tumor cell survival [14]. However, its role in TME modulation, especially in macrophages, is unknown. Given

TMBIM6's calcium channel properties [13], we hypothesized it regulates macrophage polarization via Ca^{2+} homeostasis and downstream signaling, particularly the Ca^{2+}/CaM/CaMKII pathway, which inhibits M2 polarization [15].

A key question is how TMBIM6 is upregulated in NPC. Y-box binding protein 1 (YBX1) is an oncogenic RNA-binding protein [16] that acts as an m5C modification "reader," stabilizing target mRNAs [17, 18]. Bioinformatics predicted YBX1 binds TMBIM6 mRNA. Additionally, TRIM24, an E3 ubiquitin ligase, has context-dependent functions; its loss suppresses M1 polarization and promotes NPC [19], but whether TRIM24 regulates M2 polarization via YBX1 is unclear.

This study investigates whether TRIM24 mediates ubiquitin-dependent degradation of YBX1, reducing YBX1's m5C modification and stabilization of TMBIM6 mRNA, thereby inhibiting Ca^{2+}/CaM/CaMKII signaling and blocking M2 polarization to suppress NPC. Our findings provide new insights into NPC TME formation and support combination immunotherapies targeting tumor-immune interactions.

Results

TMBIM6 is Highly Expressed in NPC and Correlates with M2 Macrophage Infiltration

We first assessed TMBIM6 expression in clinical NPC samples. Compared to non-cancerous nasopharyngeal tissues, both mRNA and protein levels of TMBIM6 were significantly upregulated in NPC tissues (Fig. 1A, B). Analysis of the tumor microenvironment revealed elevated protein expression of M2 macrophage markers (CD206, TGF-β1) and decreased expression of M1 markers (CD86, iNOS) in NPC tissues (Fig. 1C), indicating that high TMBIM6 expression is associated with an immunosuppressive microenvironment enriched with M2 macrophages.

To verify at the cellular level, we polarized THP-1 cells into M0, M1, and M2 macrophages. qPCR and ELISA confirmed successful induction of M1 (TNF-α, iNOS, IL-6) and M2 (CD206, IL-10, Arg-1) phenotypes (Fig. 1D, E). Notably, TMBIM6 expression was significantly higher in M2 macrophages compared to M0 and M1 macrophages (Fig. 1F), suggesting its specific involvement in M2 polarization.

Knockdown of TMBIM6 Inhibits M2 Macrophage Polarization and Impairs Its Pro-Tumor Functions

To investigate TMBIM6 function, we stably knocked down TMBIM6 in THP-1 cells using shRNA (Fig. 2A, B) and induced their differentiation into M2 macrophages. TMBIM6 knockdown led to upregulation of M1 markers (TNF-α, iNOS, IL-6) and downregulation of M2 markers (CD206, IL-10, Arg-1) (Fig. 2C, D). Flow cytometry further confirmed that TMBIM6 knockdown decreased the CD206-positive rate and increased the CD86-positive rate on the surface of M2 macrophages (Fig. 2E), indicating that TMBIM6 is necessary for maintaining the M2 phenotype.

Next, we examined the effect of macrophage TMBIM6 expression on NPC cell behavior. Co-culturing NPC cells (5-8F, C666-1) with conditioned medium from TMBIM6-knockdown M2 macrophages significantly inhibited NPC cell viability (CCK-8, Fig. 2F), proliferation (EdU, Fig. 2G), migration (Fig. 2H), and invasion (Fig. 2I). This suggests that macrophages promote malignant phenotypes of NPC cells via a TMBIM6-dependent pathway.

TMBIM6 Regulates M2 Polarization via Suppressing the Ca^{2+}/CaM/CaMKII Pathway

Mechanistically, we found that TMBIM6 knockdown significantly increased intracellular calcium ion (Ca^{2+}) concentration in M2 macrophages (Fig. 3A) and activated calmodulin (CaM) and its downstream effector phospho-CaMKII (p-CaMKII) (Fig. 3B). Treatment with the CaMKII-specific inhibitor KN93 reversed the increased Ca^{2+} influx (Fig. 3C) and the upregulation of CaM/p-CaMKII (Fig. 3D) caused by TMBIM6 knockdown. More importantly, KN93 treatment also completely reversed the effects of TMBIM6 knockdown on macrophage polarization markers (Fig. 3E, F) and surface phenotype (Fig. 3G). This demonstrates that TMBIM6 promotes M2 macrophage polarization by inhibiting the activation of the Ca^{2+}/CaM/CaMKII pathway.

YBX1 Positively Regulates TMBIM6 Expression via m5C Modification

To explore the upstream mechanism regulating TMBIM6 expression, we investigated the RNA-binding protein YBX1. Clinical sample analysis showed that YBX1 was also highly expressed in NPC tissues, and its expression level was significantly positively correlated with TMBIM6 (Fig. 4A-C). In macrophages, YBX1 expression was higher in M2 than in M1 type (Fig. 4D, E). Knockdown of YBX1 significantly reduced both mRNA and protein levels of TMBIM6 (Fig. 4F, G). Mechanistically, MeRIP-qPCR experiments showed that YBX1 knockdown decreased the m5C modification level of *TMBIM6* mRNA (Fig. 4H). Actinomycin D chase assays revealed that YBX1 knockdown accelerated the degradation of *TMBIM6* mRNA (Fig. 4I). Dual-luciferase reporter assays further confirmed that YBX1 enhances *TMBIM6* expression by binding to a specific site in its 3'UTR (Fig. 4J). These results demonstrate that YBX1 positively regulates TMBIM6 expression by enhancing m5C modification and stability of its mRNA.

YBX1 Affects Macrophage Polarization and NPC Progression by Regulating TMBIM6

Functional rescue experiments showed that overexpression of TMBIM6 in YBX1-knockdown M2 macrophages partially restored the decrease in TMBIM6 expression caused by YBX1 loss (Fig. 5A, B), as well as the increased intracellular Ca^{2+} levels and upregulated CaM/p-CaMKII (Fig. 5C, D). Simultaneously, TMBIM6 overexpression also reversed the M2 polarization inhibition phenotype (Fig. 5E-G) and the inhibitory effects on NPC cell proliferation, migration, and invasion caused by YBX1

knockdown (Fig. 6A-D). This establishes YBX1 as an upstream regulator of TMBIM6, influencing downstream biological processes through TMBIM6.

TRIM24 Acts as an E3 Ubiquitin Ligase Targeting YBX1 for Degradation

We further investigated the upstream regulator of YBX1. Bioinformatics prediction and co-immunoprecipitation (Co-IP) confirmed a direct interaction between the E3 ubiquitin ligase TRIM24 and YBX1 (Fig. 7A, B). Overexpression of TRIM24 did not affect YBX1 mRNA levels but significantly decreased its protein level and shortened its half-life (Fig. 7C-E). Importantly, TRIM24 overexpression enhanced polyubiquitination of YBX1 (Fig. 7F). These results demonstrate that TRIM24 degrades YBX1 via the ubiquitin-proteasome pathway, thereby negatively regulating downstream TMBIM6 expression.

Targeting the TMBIM6 Axis Synergizes with PD-L1 Inhibitor to Suppress Tumor Growth In Vivo

Finally, we validated the therapeutic potential of this pathway in a nude mouse subcutaneous xenograft model. Compared to the control group, conditioned medium from TMBIM6-knockdown M2 macrophages significantly inhibited tumor growth (Fig. 8A-C, **Supplementary Table 3**). Histological analysis showed reduced tumor cell proliferation (Ki67) and increased apoptosis (TUNEL) in this group (Fig. 8F, G). Combination with a PD-L1 inhibitor further enhanced tumor suppression, showing a significant synergistic effect (Fig. 8A-G). Analysis of tumor tissues confirmed the highest activation level of CaM/p-CaMKII in the combination treatment group (Fig. 8E), consistent with the in vitro mechanism.

Discussion

This study systematically delineates and validates a comprehensive signaling axis in NPC that uniquely connects protein ubiquitination, RNA epitranscriptomic modification, ion signaling, and immune cell functional remodeling: TRIM24 --| (ubiquitination degradation) YBX1 --| (m5C modification-mediated mRNA stabilization) TMBIM6 --| (inhibition) Ca^{2+}/CaM/CaMKII pathway --| (blockade) M2 macrophage polarization (Fig. 9). Elucidating this multi-layered regulatory network not only provides an innovative theoretical framework for understanding the formation of the immunosuppressive TME in NPC but also reveals multiple molecular targets with potential therapeutic value.

First, this study discovers and establishes a novel central function for TMBIM6 in regulating the tumor immune microenvironment. Previous research on TMBIM6 has focused almost exclusively on its role in tumor cells themselves, conferring resistance to ER stress and apoptosis [13, 14]. Our work extends the functional scope of TMBIM6 to the interaction between tumor cells and immune cells, particularly macrophages. We found that TMBIM6 is specifically highly expressed in M2 macrophages, and its functional loss does not directly kill tumor cells but rather "reprograms" macrophages, shifting them

from a pro-tumor M2 phenotype towards an anti-tumor M1 phenotype, thereby indirectly inhibiting tumors. This finding aligns with the research trend emphasizing "non-cell-autonomous" oncogenic mechanisms within the TME [12, 9]. Our study opens a new direction for understanding TMBIM6's oncogenic mechanism, demonstrating that it drives tumor progression not only through intrinsic cell survival mechanisms but also by shaping an immunosuppressive microenvironment, providing a more comprehensive perspective on its overexpression in various cancers.

Second, this study elucidates the precise molecular mechanism by which TMBIM6 regulates macrophage polarization, namely through inhibition of the Ca^{2+}/CaM/CaMKII signaling pathway. Mechanistic exploration is key to understanding its function. Based on TMBIM6's calcium channel properties [13], we found that its knockdown triggered "calcium leakage" in macrophages, leading to elevated cytosolic Ca^{2+} levels. This change unexpectedly activated the Ca^{2+}/CaM/CaMKII pathway, typically associated with pro-inflammatory (M1) responses [15, 20, 21]. This finding resonates with the work of Cai et al., which showed that MerTK signaling promotes inflammation resolution (associated with M2 function) by suppressing CaMKII activity [21], collectively highlighting CaMKII activity as a key switch in macrophage polarization. Rescue experiments using the specific inhibitor KN93 perfectly confirmed the causal role of this pathway. Therefore, our data reveal a novel model: in the NPC microenvironment, highly expressed TMBIM6 constitutively inhibits the Ca^{2+}/CaM/CaMKII pathway by maintaining lower calcium levels in macrophages, thereby creating a "permissive" intracellular environment for M2 polarization. This provides an important paradigm for understanding how tumors achieve immune cell "reprogramming" and immune escape through precise regulation of ionic homeostasis [22, 23, 24].

Third, we reveal for the first time the upstream post-transcriptional regulatory mechanism for TMBIM6 overexpression in NPC, namely YBX1-mediated m5C-dependent mRNA stabilization. To address the fundamental question of "why TMBIM6 is highly expressed in NPC," we focused on the RNA-binding protein YBX1. We not only confirmed the positive correlation between YBX1 and TMBIM6 but, more importantly, through a series of experiments, clarified that YBX1 enhances TMBIM6 mRNA stability and upregulates its expression by recognizing and binding to m5C modification sites on its 3'UTR. m5C modification is a hotspot in tumor epitranscriptomics research [17, 18]. Our work successfully links the "YBX1-m5C-TMBIM6" regulatory module directly to the formation of the immunosuppressive tumor microenvironment, expanding the functional understanding of RNA modifications in tumor immunoregulation. This parallels the study by Wang et al., which found that the NSUN2/YBX1 axis mediates EGFR-TKI resistance in lung cancer via m5C modification [18], suggesting the universality of the YBX1-m5C regulatory axis in tumor malignant phenotypes. Our study is the first to localize its function to immune microenvironment remodeling.

Fourth, this study identifies the "master switch" regulating the upstream part of this pathway—the E3 ubiquitin ligase TRIM24, which exerts negative regulation by targeting YBX1 for degradation. The role of TRIM24 in cancer exhibits tissue specificity and context dependency [19]. We confirmed that TRIM24 is an E3 ubiquitin ligase for YBX1, promoting its degradation, leading to decreased downstream TMBIM6

expression and inhibited M2 polarization. This finding provides a novel molecular explanation for the potential tumor-suppressive function of TRIM24 in specific contexts, such as the NPC immune microenvironment [19]. This forms an interesting contrast with the traditional role of TRIM24 as an oncogene in certain cancers, highlighting the significant influence of tumor microenvironmental context on E3 ligase function. More importantly, our research unveils a coherent regulatory chain from protein post-translational modification (ubiquitination) to RNA post-transcriptional modification (m5C-mediated stabilization), to ion signaling and cellular functional phenotypes, providing an example for understanding the integration of multi-level regulatory networks in tumors.

Finally, the in vivo data from this study hold clear clinical translational prospects. We found that the "macrophage reprogramming" strategy based on TMBIM6 knockdown effectively inhibited tumor growth in a nude mouse model. Particularly important, this strategy showed synergistic efficacy when combined with a PD-L1 inhibitor. This suggests that targeting TMBIM6 or its pathway may have dual therapeutic value: first, directly relieving the drive for M2 polarization and reversing immunosuppression; second, potentially converting immunosuppressive "cold tumors" into "hot tumors" more sensitive to immune checkpoint inhibitors by altering cytokine profiles and immune cell composition within the microenvironment [10, 25], thereby offering a potential approach to overcome prevalent primary or acquired resistance in current immunotherapy [8, 25]. This provides strong experimental rationale for developing novel combination immunotherapies.

This study has several limitations. Mechanistically, the specific domains mediating TRIM24-YBX1 interaction and the precise structural basis for YBX1's recognition of m5C sites on TMBIM6 mRNA require further investigation. Our conclusions are primarily based on cell lines and immunodeficient mouse models; validation in patient-derived organoids and humanized models is needed to assess this pathway in the context of adaptive immunity. While we propose TMBIM6 as a therapeutic target, effective small-molecule inhibitors remain to be developed. Clinical relevance could be strengthened by larger multi-center cohorts correlating pathway components with patient outcomes and immune infiltration. Additionally, whether this axis affects other immune cells (T cells, NK cells) or functions in tumor cells themselves warrants exploration.

The nude mouse model allowed focused study of macrophage polarization but lacks adaptive immune components, limiting full assessment of combination PD-L1 therapy. The observed synergy may reflect a microenvironment remodeled by TMBIM6 targeting (reduced M2 macrophages) creating conditions favorable for other effectors. Future validation in humanized or immunocompetent models will enable comprehensive evaluation of therapeutic efficacy and anti-tumor T-cell immunity.

In summary, this study identifies a key signaling axis in NPC that unprecedentedly multi-layeredly regulates macrophage polarization and tumor progression. This axis initiates with TRIM24-mediated ubiquitin-dependent degradation of YBX1, proceeds through downregulation of YBX1's m5C modification and stabilization of *TMBIM6* mRNA, ultimately inhibiting the Ca^{2+}/CaM/CaMKII pathway, thereby blocking macrophage polarization towards the immunosuppressive M2 phenotype. This work not only deepens

the understanding of the mechanisms underlying NPC immunosuppressive microenvironment formation but also links several cutting-edge fields including protein homeostasis, RNA epigenetics, ion signaling, and tumor immunology. Targeting key nodes within this pathway, particularly TMBIM6, provides a highly promising new direction and novel targets for developing combination therapeutic strategies capable of reversing immunosuppression and enhancing the efficacy of existing immunotherapies.

Materials and Methods

Study Design and Ethical Compliance

This mechanistic investigation combined analysis of clinical specimens, in vitro molecular and cellular assays, and preclinical animal studies. The human sample component was designed as a retrospective observational analysis. In contrast, the animal studies followed a randomized, controlled intervention protocol.

For research involving human tissues, the study protocol adhered strictly to the principles of the Declaration of Helsinki. Approval was granted by the Ethics Review Committee of the First Affiliated Hospital, University of South China (Approval No.: 2024LL0510002). The committee waived the requirement for individual written informed consent as the project utilized only de-identified, residual diagnostic tissue archives. This decision was consistent with national guidelines on ethical review for biomedical research involving human subjects and Article 32 of the Declaration of Helsinki, considering the minimal risk involved.

All procedures involving laboratory animals were conducted in compliance with China's Regulations on the Management of Laboratory Animals and the international ARRIVE 2.0 guidelines. The Institutional Animal Care and Use Committee (IACUC) at the First Affiliated Hospital, University of South China, reviewed and approved the protocols (Approval No.: 2024LL0510002).

Processing of Clinical Specimens

Pathological biopsy samples were obtained from 20 patients newly diagnosed with NPC at our institution between June and November 2024. For comparison, nasopharyngeal tissues were also collected from 10 individuals without cancer. Key inclusion criteria were: 1) histopathological confirmation of NPC or its absence; 2) no evidence of distant metastasis prior to or during initial treatment; 3) no previous history of anticancer therapy; and 4) absence of other malignancies. Primary exclusion criteria included suspected or confirmed distant metastasis, concurrent severe infections or major systemic illnesses, and a history of other cancers. Demographic characteristics, including age and gender, showed no significant difference between the NPC and control groups (see **Supplementary Table 1** for details).

Immediately following resection, each fresh tissue sample was divided. One portion was fixed in 4% paraformaldehyde for standard paraffin embedding, subsequent histological evaluation (H&E staining),

EBER in situ hybridization, and immunohistochemical (IHC) analysis. The remaining portion was snap-frozen in liquid nitrogen and stored at -80°C for later extraction of proteins and total RNA. Paraffin-embedded samples were excluded from molecular biology assays due to potential nucleic acid degradation.

Cell Culture Protocols

The human monocytic cell line THP-1 and two NPC cell lines, 5-8F and C666-1 (a well-differentiated line), were acquired from Hunan Fenghui Biotechnology Co., Ltd. All cell lines were confirmed mycoplasma-free. THP-1 cells were maintained in suspension culture using RPMI-1640 medium (Gibco, 12800017) supplemented with 10% heat-inactivated fetal bovine serum (FBS, Gibco, 10099141), penicillin (100 U/mL), and streptomycin (100 µg/mL). The adherent NPC cell lines (5-8F and C666-1) were cultured in DMEM high-glucose medium (Gibco, 12800017) containing the same concentration of FBS and antibiotics. Cultures were incubated at 37°C in a humidified atmosphere with 5% CO_2.

Induction and Polarization of Macrophages

To generate non-polarized M0 macrophages, THP-1 cells in logarithmic growth phase were plated at 5 x 10^5 cells/mL and treated with 100 nM phorbol 12-myristate 13-acetate (PMA, Sigma) for 48 hours. The adherent, spindle-shaped cells were then rested in fresh complete medium for 24 hours to stabilize the M0 phenotype.

For polarization, M0 macrophages were stimulated as follows:

M1 Phenotype: Culture with medium containing 100 ng/mL lipopolysaccharide (LPS, Sigma) and 20 ng/mL interferon-γ (IFN-γ, PeproTech) for 24 hours.

M2 Phenotype: Culture with medium containing 20 ng/mL interleukin-4 (IL-4, PeproTech) and 20 ng/mL interleukin-13 (IL-13, PeproTech) for 48 hours.

The efficiency of polarization was confirmed by quantifying specific markers via qRT-PCR and flow cytometry (M1: TNF-α, iNOS, CD86; M2: CD206, Arg-1, IL-10).

Generation of Stable Cell Lines via Lentiviral Transduction

Short hairpin RNA (shRNA) sequences targeting human TMBIM6 and YBX1, along with a TRIM24 overexpression construct, were designed and synthesized by Shanghai GenePharma Co., Ltd. A non-targeting scrambled shRNA sequence served as the negative control (sh-NC). These sequences were cloned into the pLKO.1-puro (for knockdown) or pLVX-puro (for overexpression) vectors. Lentiviral particles were produced in 293T cells using a standard three-plasmid packaging system, and the viral supernatants were harvested and concentrated.

To establish stable lines, THP-1-derived M0 macrophages were transduced with lentivirus at a multiplicity of infection (MOI) of 50, using Polybrene (8 µg/mL) to enhance efficiency. Seventy-two hours post-transduction, cells were selected with 2.5 µg/mL puromycin (Sigma) for a minimum of 7 days.

Successful knockdown or overexpression was verified by observing green fluorescent protein (GFP) fluorescence (encoded by the vector) and by Western blot analysis.

RNA Analysis and Quantitative Real-Time PCR (qRT-PCR)

Total RNA was isolated using TRIzol® Reagent (Invitrogen). RNA concentration and purity (A260/A280 ratio of 1.8-2.0) were determined with a NanoDrop 2000 spectrophotometer (Thermo Scientific). One microgram of total RNA was first treated with a gDNA Eraser, followed by reverse transcription using the PrimeScript™ RT reagent Kit (Takara). qPCR was performed on an Applied Biosystems 7500 Real-Time PCR System with SYBR® Premix Ex Taq™ II (Takara). The thermal cycling protocol consisted of an initial denaturation at 95°C for 30 seconds, followed by 40 cycles of 95°C for 5 seconds and 60°C for 34 seconds. β-actin mRNA was used as the endogenous control for normalization. Relative mRNA expression levels were calculated using the 2^(-ΔΔCt) method. All primer sequences (listed in **Supplementary Table 2**) were validated for specificity and synthesized by Sangon Biotech (Shanghai).

Protein Extraction and Immunoblotting

Cells or tissue samples were lysed on ice using pre-chilled RIPA lysis buffer (Beyotime) containing 1% phenylmethylsulfonyl fluoride (PMSF) protease inhibitor for 30 minutes. Lysates were centrifuged at 12,000 × g for 15 minutes at 4°C to collect the supernatant. Protein concentration was quantified with a BCA protein assay kit (Beyotime). Equal amounts of protein (20–30 μg) were resolved by 10% SDS-PAGE and electrophoretically transferred to polyvinylidene difluoride (PVDF) membranes (Merck Millipore).

After blocking with 5% non-fat milk for one hour at room temperature, membranes were probed with primary antibodies overnight at 4°C. The following primary antibodies and dilutions were used: TMBIM6 (Biorbyt, orb1184701, 1:1000), YBX1 (Abcam, ab76149, 1:1000), TRIM24 (Thermo, A300-815A-T, 1:1000), CaM (Thermo, MA3-917, 1:500), CaMKII (Thermo, MA1-048, 1:1000), phospho-CaMKII (Thr286) (Thermo, MA1-047, 1:2000), CD206 (Thermo, MA5-32498, 1:2000), iNOS (Abcam, ab178945, 1:1000), β-actin (Abcam, ab8226, 1:5000). Following washes, membranes were incubated with appropriate horseradish peroxidase (HRP)-conjugated secondary antibodies (1:5000) for one hour at room temperature. Protein bands were visualized using Super ECL chemiluminescent substrate (GENVIEW) on a ChemiScope 6000 imaging system (Qinxiang), and band intensities were quantified with ImageJ software, normalized to β-actin.

Co-Immunoprecipitation (Co-IP) and Ubiquitination Assay

To examine the interaction between TRIM24 and YBX1, THP-1 cells overexpressing TRIM24 were lysed on ice with NP-40 lysis buffer (Beyotime). For each immunoprecipitation, 500 μg of total protein was incubated with 2 μg of anti-TRIM24 antibody or an equivalent amount of control IgG overnight at 4°C with gentle rotation. Protein A/G agarose beads (Thermo), pre-equilibrated with lysis buffer, were then added, and the incubation continued for an additional 4 hours. The beads were washed five times with cold lysis buffer, and the bound proteins were eluted by boiling in 1× SDS loading buffer for 10 minutes before analysis by Western blot.

To detect YBX1 ubiquitination, cells were pre-treated with the proteasome inhibitor MG132 (10 μM, MCE) for 6 hours prior to lysis. Cell lysis was performed with buffer containing 1% SDS, followed by boiling for 10 minutes to disrupt non-covalent protein interactions. The lysate was then diluted 10-fold with regular NP-40 lysis buffer to reduce the SDS concentration. Subsequent Co-IP steps were carried out using an anti-YBX1 antibody, and ubiquitinated YBX1 was detected by immunoblotting with an anti-ubiquitin antibody (Abcam, ab140601, 1:1000).

Detection of RNA Methylation (MeRIP-qPCR)

The Magna MeRIP™ m5C Kit (Merck Millipore) was employed according to the manufacturer's protocol. Briefly, total RNA extracted from THP-1 cells was fragmented into 100–300 nucleotide pieces. A small aliquot of fragmented RNA was saved as the input control. The remainder was incubated overnight at 4°C with rotation in IP buffer containing either an anti-m5C antibody (Synaptic Systems, 202003) or normal mouse IgG. Immune complexes were captured with Protein A/G magnetic beads. The enriched RNA was eluted, purified, and subjected to reverse transcription and qPCR alongside the input RNA to determine the enrichment of TMBIM6 mRNA. Enrichment was calculated as 2^[Ct(IgG) - Ct(m5C-IP)].

Dual-Luciferase Reporter Assay

DNA fragments corresponding to the wild-type (WT) 3' untranslated region (UTR) of the TMBIM6 gene, containing a predicted YBX1 binding site, and a mutant (MUT) version with point mutations in this site were synthesized and cloned into the pmirGLO dual-luciferase reporter vector (Promega). PMA-induced THP-1 cells, seeded in 24-well plates, were co-transfected with 400 ng of the reporter construct and either a YBX1 overexpression plasmid or an empty control vector. After 48 hours, cells were lysed, and firefly and Renilla luciferase activities were measured sequentially using the Dual-Luciferase® Reporter Assay System (Promega) on a GloMax® 20/20 luminometer (Promega). Relative luciferase activity was calculated by normalizing firefly luminescence to Renilla luminescence.

Assessment of mRNA Stability

M2 macrophages with stable YBX1 knockdown or control cells were treated with the transcriptional inhibitor actinomycin D (ActD, Sigma) at a final concentration of 5 μg/mL. Cells were harvested at 0, 2, 4, and 8 hours post-treatment for total RNA extraction. The relative abundance of TMBIM6 mRNA at each time point was determined by qRT-PCR and normalized to β-actin. The value at the 0-hour time point was set to 1, and an mRNA decay curve was plotted.

Flow Cytometric Analyses

For surface marker detection, treated macrophages were collected, resuspended in Cell Staining Buffer (Biolegend), and incubated with fluorescein isothiocyanate (FITC)-conjugated anti-human CD86 (Thermo, MA1-10293) and phycoerythrin (PE)-conjugated anti-human CD206 (Thermo, MA5-32498) antibodies on ice in the dark for 30 minutes. After washing, cells were analyzed on a Beckman CytoFLEX flow cytometer, and data were processed using FlowJo V10 software.

To measure intracellular Ca^{2+} concentration, cells were loaded with 2 μM Fluo-4 AM calcium indicator (Beyotime) for 30 minutes at 37°C, washed, and analyzed immediately by flow cytometry. The mean fluorescence intensity (MFI) was used to represent relative Ca^{2+} levels.

Functional Assays on NPC Cells

Proliferation and Viability (CCK-8): NPC cells were plated in 96-well plates at 2000 cells/well and co-cultured with various conditioned media. At designated time points, 10 μL of CCK-8 solution (Elabscience) was added to each well. After 2 hours of incubation, the absorbance at 450 nm was measured with a microplate reader (Thermo Labsystems).

Proliferation (EdU Assay): Cells were incubated with 50 μM 5-ethynyl-2'-deoxyuridine (EdU) for 2 hours using the Click-iT™ EdU Imaging Kit (Invitrogen). After fixation and permeabilization, the Click-iT reaction (with Alexa Fluor 488 azide) was performed to label incorporated EdU, and nuclei were counterstained with Hoechst 33342. The percentage of EdU-positive (green) nuclei among total (blue) nuclei was calculated from images of five random fields captured under a fluorescence microscope.

Migration and Invasion (Transwell): Transwell chambers with 8 μm pores (Corning) were used. For migration assays, 5 x 10^4 NPC cells in serum-free medium were seeded in the upper chamber. For invasion assays, the upper chamber membrane was pre-coated with Matrigel (50 μg/chamber, BD Biosciences), and 1 x 10^5 cells were seeded. The lower chamber contained complete medium with 10% FBS as a chemoattractant. After 24 hours (migration) or 48 hours (invasion), non-migrated/invaded cells on the upper side of the membrane were removed. Cells that had traversed the membrane were fixed with 4% paraformaldehyde, stained with 0.1% crystal violet, and counted in five random fields (200x magnification) under a light microscope (Nikon Eclipse Ti).

Animal Studies In Vivo

All animal procedures followed ARRIVE 2.0 guidelines and were approved by the Animal Ethics Committee of the First Affiliated Hospital, University of South China (2024LL0510002). Male BALB/c nude mice (5 weeks, 18.5 ± 0.5 g) were obtained from Hunan Slake Jingda [SCXK (Xiang) 2023-0004] and acclimatized for one week in an SPF facility [SYXK (Xiang) 2023-0010]. Mice were housed in IVC cages (≤ 5/cage) at 22 ± 1°C, 55 ± 5% humidity, with a 12 h light/dark cycle and free access to irradiated food and sterile water.

Sample size was determined by power analysis (G*Power 3.1: d = 2.0, α = 0.05, power = 80%, n = 4/group). Twenty mice were stratified by weight and randomly allocated into five groups (n = 4): (1) Control (C666-1 + Matrigel); (2) M2-CM (C666-1 + normal M2 macrophage CM); (3) shNC-M2-CM (C666-1 + shRNA control M2 CM); (4) shTMBIM6-M2-CM (C666-1 + TMBIM6-knockdown M2 CM); (5) shTMBIM6-M2-CM + αPD-L1 (same as group 4 plus anti-PD-L1). Blinding was maintained for all procedures until data collection.

C666-1 cells pre-conditioned with corresponding CM were mixed with Matrigel (BD Biosciences) and injected subcutaneously (1×10^6 cells/mouse). Group 5 received i.p. anti-PD-L1 (10 mg/kg, clone 10F.9G2, BioXcell, BE0101) every 3 days starting day 2; other groups received PBS. Tumor volume ($V = L\times W^2/2$) and body weight were monitored every 4 days. Humane endpoints included tumor > 2000 mm^3, ulceration > 10 mm, > 20% weight loss, or severe distress. At day 28, mice were euthanized by CO_2, tumors excised, weighed, and bisected for protein analysis and histology.

Euthanasia was performed by CO_2 asphyxiation using a compressed CO_2 cylinder connected to a flow regulator, with a fill rate of approximately 20% of the chamber volume per minute, consistent with the AVMA Guidelines for the Euthanasia of Animals. Death was confirmed by respiratory arrest and lack of pedal reflex, followed by cervical dislocation as a secondary method to ensure death.

Histology and Immunohistochemistry (IHC)

For IHC, paraffin sections were stained with anti-Ki67 (Abcam, ab15580, 1:200) and DAB. Apoptosis was detected by TUNEL (Roche). Positive cells were counted in five random fields (400×). Apoptosis was detected using the In Situ Cell Death Detection Kit, TMR red (Roche), according to the manufacturer's instructions (TUNEL assay).

Statistical Analysis

In vitro experiments were performed in at least three independent replicates. Data are expressed as mean ± standard deviation (SD). Statistical analyses were conducted with GraphPad Prism 8.0 software. Comparisons between two groups were made using an unpaired, two-tailed Student's t-test. For comparisons among multiple groups, one-way analysis of variance (ANOVA) was applied. If ANOVA assumptions (homogeneity of variances) were met, Tukey's test was used for post-hoc multiple comparisons. If variances were unequal, Welch's ANOVA followed by Dunnett's T3 test was employed. A P-value of less than 0.05 was considered statistically significant (*$P < 0.05$, **$P < 0.01$, ***$P < 0.001$).

Abbreviations

Calmodulin (CaM); Ca^{2+}/calmodulin-dependent protein kinase II (CaMKII); Cell Counting Kit-8 (CCK-8); Conditioned Medium (CM); Co-Immunoprecipitation (Co-IP); Epstein-Barr Virus (EBV); 5-Ethynyl-2´-deoxyuridine (EdU); Endoplasmic Reticulum (ER); Fetal Bovine Serum (FBS); Hematoxylin and Eosin (H&E); Institutional Animal Care and Use Committee (IACUC); Immune Checkpoint Inhibitors (ICIs); Interferon-gamma (IFN-γ); Immunohistochemistry (IHC); Interleukin-4/10/13 (IL-4/10/13); Inducible Nitric Oxide Synthase (iNOS); Lipopolysaccharide (LPS); 5-Methylcytosine (m5C); Methylated RNA Immunoprecipitation followed by qPCR (MeRIP-qPCR); Mean Fluorescence Intensity (MFI); Multiplicity of Infection (MOI); Mutant (MUT); Nasopharyngeal Carcinoma (NPC); Phosphate-Buffered Saline (PBS); Programmed Death-Ligand 1 (PD-L1); Phorbol 12-myristate 13-acetate (PMA); Quantitative Real-Time Polymerase Chain Reaction (qRT-PCR); Short Hairpin RNA (shRNA); Specific Pathogen-Free (SPF); Tumor-Associated Macrophages (TAMs); Transmembrane Bax Inhibitor Motif-containing 6 (TMBIM6); Tumor Microenvironment (TME); Tripartite Motif-containing 24 (TRIM24); Terminal deoxynucleotidyl

transferase dUTP nick-end labeling (TUNEL); Western Blotting (WB); Wild Type (WT); Y-box Binding Protein 1 (YBX1).

Declarations

Acknowledgements

We thank our institute's Core Facility Center and Laboratory Animal Center for their help and mice breeding.

Funding Information

This work was supported by the Natural Science Foundation of Hunan Province [Grant Number 2026JJ80198] and the Doctoral Startup Fund of the First Affiliated Hospital of University of South China.

Conflict of Interest

The authors declare that they have no competing interests.

Author Contributions

D.Y. conceived the original idea and wrote the proposal. Y.L. and D.Y. designed the study. Y.L., Z.Y.L, J.Y.H., C.J.C., A.T.N. and Y.L. organized the data collection and analyzed the data. Y.L. and D.Y. performed the statistical analysis and wrote the manuscript for publication. All authors read and approved the final manuscript.

Data Availability Statement

The datasets generated and/or analyzed during the current study are available from the corresponding author on reasonable request. No high-throughput sequencing, proteomics, or structural data were generated, and therefore no data have been deposited in public repositories.

Ethics Approval

This study was conducted in accordance with the Helsinki Declaration and approved by the Ethics Committee of the First Affiliated Hospital of the University of South China (Approval No.: 2024LL0510002). The Ethics Committee of The First Affiliated Hospital of University of South China granted a formal waiver of written informed consent based on compliance with Article 15 of China's Regulations on Human Genetic Resources (State Council Order No. 717) and Paragraph 32 of the Declaration of Helsinki (2013). This decision was made because: (i) The study exclusively utilized deidentified residual pathological specimens obtained during routine diagnostic procedures; (ii) The research posed no additional risks to participants beyond standard care; (iii) Retrospective consent acquisition was impracticable without compromising patient confidentiality.

All animal experiments were approved by the same ethics committee and followed the ARRIVE guidelines. Our institution operates a centralized ethics review system where a single Institutional Ethics Committee (IEC) oversees all human and animal research. The approval number 2024LL0510002 covers two integrated protocols under one project: Human protocol: Use of anonymized biopsy tissues (Waiver granted); Animal protocol: Xenograft experiments. This practice is documented in Article 26 of China's Ethical Review Measures for Biomedical Research Involving Humans (NHFPC Order No. 11).

Consent for Publication

Not applicable

References

1. Sung H, Ferlay J, Siegel RL, et al. Global Cancer Statistics 2020: GLOBOCAN Estimates of Incidence and Mortality Worldwide for 36 Cancers in 185 Countries. CA Cancer J Clin. 2021;71(3):209-249. doi:10.3322/caac.21660.
2. Wei KR, Zheng RS, Zhang SW, Liang ZH, Li ZM, Chen WQ. Nasopharyngeal carcinoma incidence and mortality in China, 2013. Chin J Cancer. 2017;36(1):90. Published 2017 Nov 9. doi:10.1186/s40880-017-0257-9.
3. Chen YP, Chan ATC, Le QT, Blanchard P, Sun Y, Ma J. Nasopharyngeal carcinoma. Lancet. 2019;394(10192):64-80. doi:10.1016/S0140-6736(19)30956-0.
4. Li YQ, Tian YM, Tan SH, et al. Prognostic Model for Stratification of Radioresistant Nasopharynx Carcinoma to Curative Salvage Radiotherapy. J Clin Oncol. 2018;36(9):891-899. doi:10.1200/JCO.2017.75.5165.
5. Hsu C, Lee SH, Ejadi S, et al. Safety and Antitumor Activity of Pembrolizumab in Patients With Programmed Death-Ligand 1-Positive Nasopharyngeal Carcinoma: Results of the KEYNOTE-028 Study. J Clin Oncol. 2017;35(36):4050-4056. doi:10.1200/JCO.2017.73.3675.
6. Hsu MC, Hsiao JR, Chang KC, et al. Increase of programmed death-1-expressing intratumoral CD8 T cells predicts a poor prognosis for nasopharyngeal carcinoma. Mod Pathol. 2010;23(10):1393-1403. doi:10.1038/modpathol.2010.130.
7. Lee AWM, Ng WT, Chan JYW, et al. Management of locally recurrent nasopharyngeal carcinoma. Cancer Treat Rev. 2019;79:101890. doi:10.1016/j.ctrv.2019.101890.
8. Johnson D, Ma BBY. Targeting the PD-1/ PD-L1 interaction in nasopharyngeal carcinoma. Oral Oncol. 2021;113:105127. doi:10.1016/j.oraloncology.2020.105127.
9. Mantovani A, Allavena P, Sica A, Balkwill F. Cancer-related inflammation. Nature. 2008;454(7203):436-444. doi:10.1038/nature07205.
10. Bremnes RM, Al-Shibli K, Donnem T, et al. The role of tumor-infiltrating immune cells and chronic inflammation at the tumor site on cancer development, progression, and prognosis: emphasis on

non-small cell lung cancer. J Thorac Oncol. 2011;6(4):824-833. doi:10.1097/JTO.0b013e3182037b76.

11. Gordon SR, Maute RL, Dulken BW, et al. PD-1 expression by tumour-associated macrophages inhibits phagocytosis and tumour immunity. Nature. 2017;545(7655):495-499. doi:10.1038/nature22396.
12. Hanahan D, Weinberg RA. Hallmarks of cancer: the next generation. Cell. 2011;144(5):646-674. doi:10.1016/j.cell.2011.02.013.
13. Bultynck G, Kiviluoto S, Henke N, et al. The C terminus of Bax inhibitor-1 forms a Ca2+-permeable channel pore. J Biol Chem. 2012;287(4):2544-2557. doi:10.1074/jbc.M111.275354.
14. Zhang M, Li X, Zhang Y, Zhou K. Bax inhibitor-1 mediates apoptosis-resistance in human nasopharyngeal carcinoma cells. Mol Cell Biochem. 2010;333(1-2):1-7. doi:10.1007/s11010-009-0198-y.
15. Chen K, Man Q, Miao J, et al. Kir2.1 channel regulates macrophage polarization via the Ca2+/CaMK II/ERK/NF-κB signaling pathway. J Cell Sci. 2022;135(13):jcs259544. doi:10.1242/jcs.259544.
16. Zhou LL, Ni J, Feng WT, et al. High YBX1 expression indicates poor prognosis and promotes cell migration and invasion in nasopharyngeal carcinoma. Exp Cell Res. 2017;361(1):126-134. doi:10.1016/j.yexcr.2017.10.009.
17. Chen X, Li A, Sun BF, et al. 5-methylcytosine promotes pathogenesis of bladder cancer through stabilizing mRNAs. Nat Cell Biol. 2019;21(8):978-990. doi:10.1038/s41556-019-0361-y.
18. Wang Y, Wei J, Feng L, et al. Aberrant m5C hypermethylation mediates intrinsic resistance to gefitinib through NSUN2/YBX1/QSOX1 axis in EGFR-mutant non-small-cell lung cancer. Mol Cancer. 2023;22(1):81. Published 2023 May 9. doi:10.1186/s12943-023-01780-4.
19. Liu H, Tang L, Gong S, et al. USP7 inhibits the progression of nasopharyngeal carcinoma via promoting SPLUNC1-mediated M1 macrophage polarization through TRIM24. Cell Death Dis. 2023;14(12):852. Published 2023 Dec 21. doi:10.1038/s41419-023-06368-w.
20. Bossuyt J, Bers DM. Visualizing CaMKII and CaM activity: a paradigm of compartmentalized signaling. J Mol Med (Berl). 2013;91(8):907-916. doi:10.1007/s00109-013-1060-y.
21. Cai B, Kasikara C, Doran AC, Ramakrishnan R, Birge RB, Tabas I. MerTK signaling in macrophages promotes the synthesis of inflammation resolution mediators by suppressing CaMKII activity. Sci Signal. 2018;11(549):eaar3721. Published 2018 Sep 25. doi:10.1126/scisignal.aar3721.
22. Hudmon A, Schulman H. Structure-function of the multifunctional Ca2+/calmodulin-dependent protein kinase II. Biochem J. 2002;364(Pt 3):593-611. doi:10.1042/BJ20020228.
23. Berchtold MW, Villalobo A. The many faces of calmodulin in cell proliferation, programmed cell death, autophagy, and cancer. Biochim Biophys Acta. 2014;1843(2):398-435. doi:10.1016/j.bbamcr.2013.10.021.
24. Liu Q, Zhu P, Liu S, et al. NMAAP1 Maintains M1 Phenotype in Macrophages Through Binding to IP3R and Activating Calcium-related Signaling Pathways. Protein Pept Lett. 2019;26(10):751-757. doi:10.2174/0929866526666190503105343.

25. Liu N, Zhang J, Yin M, et al. Inhibition of xCT suppresses the efficacy of anti-PD-1/L1 melanoma treatment through exosomal PD-L1-induced macrophage M2 polarization. Mol Ther. 2021;29(7):2321-2334. doi:10.1016/j.ymthe.2021.03.013.

Figures

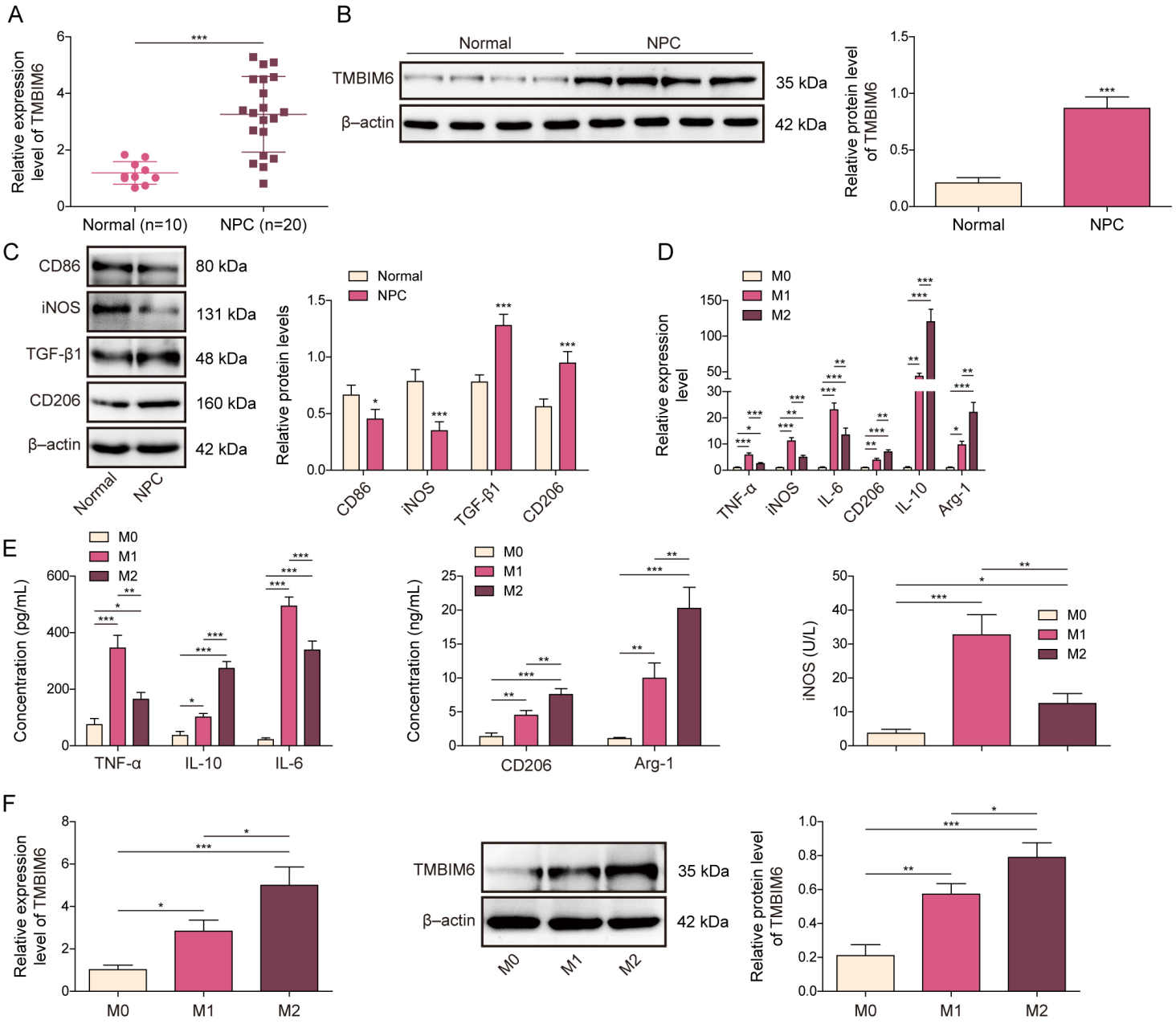

Figure 1

TMBIM6 is highly expressed in NPC tissues and M2 macrophages.

(A) Relative mRNA expression of TMBIM6 in nasopharyngeal carcinoma (NPC, n=20) and adjacent normal tissues (Normal, n=10) detected by qRT-PCR. (B) Western Blot (top) and quantitative analysis (bottom) showing TMBIM6 protein expression levels in tissues. (C) Western Blot (left) and quantitative

analysis (right) of protein expression for M1 (CD86, iNOS) and M2 (CD206, TGF-β1) macrophage markers in tissues. (D) qRT-PCR analysis of M1/M2-related factor mRNA expression in M0, M1, and M2 macrophages. (E) ELISA analysis of M1/M2-related factor protein concentration in culture supernatants of M0, M1, and M2 macrophages. (F) qRT-PCR (left) and Western Blot (right) analysis of TMBIM6 expression in macrophages under different polarization states. Data are presented as mean ± SD; *P < 0.05, **P < 0.01, ***P < 0.001 (Student's t-test or one-way ANOVA). The original blotting images are shown in Supplementary Figure 1. The grouping of these blotting images is indicated by the white lines/ intervals between the lanes.

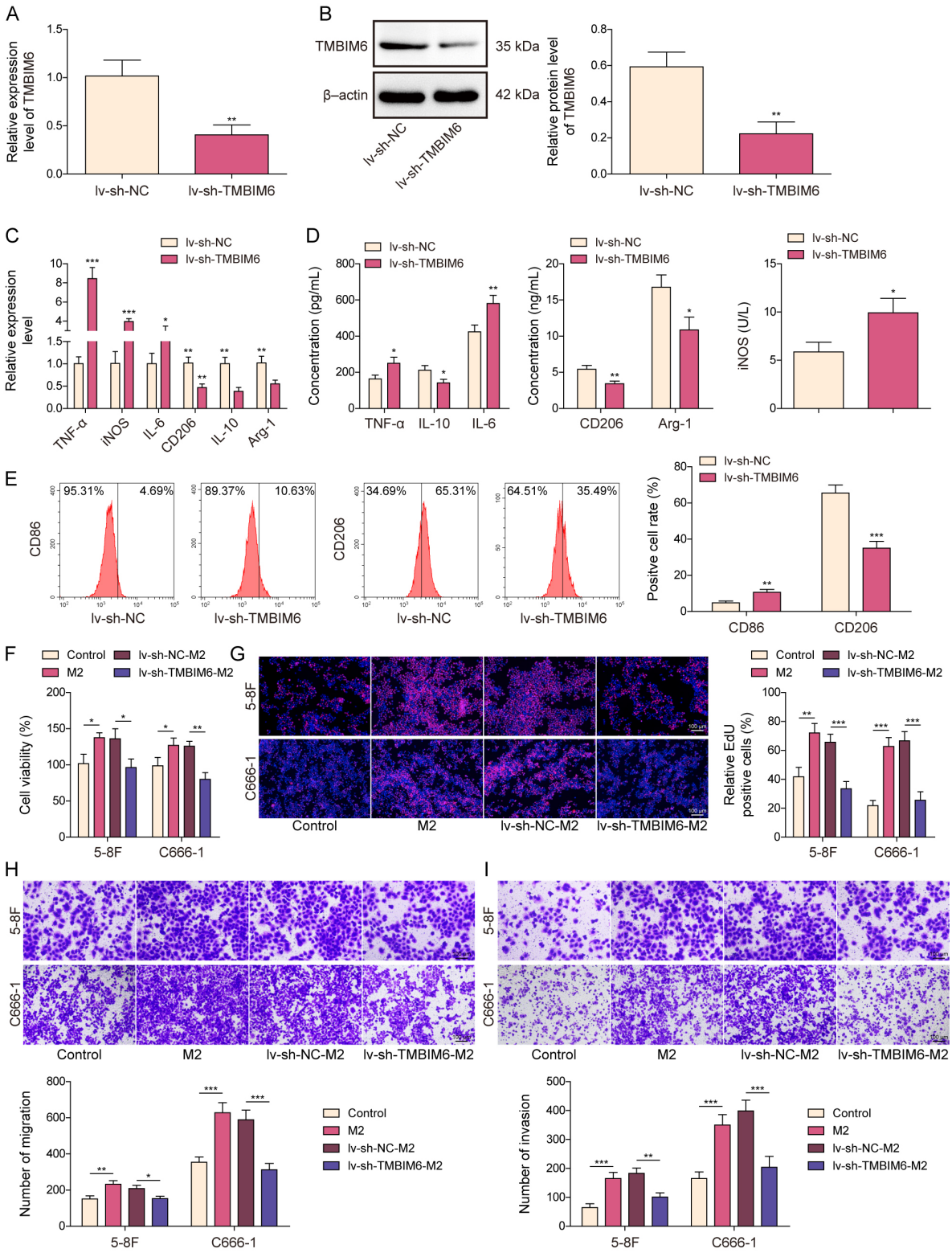

Figure 2

Knockdown of TMBIM6 inhibits M2 macrophage polarization and its pro-tumorigenic effects on NPC cells.

(A, B) qRT-PCR (A) and Western Blot (B) verification of TMBIM6 knockdown efficiency in M2 macrophages. (C, D) qRT-PCR (C) and ELISA (D) analysis of the effects of TMBIM6 knockdown on the

expression of M1/M2-related factors. (E) Flow cytometry analysis of the effect of TMBIM6 knockdown on the surface expression of CD86 and CD206 on M2 macrophages (left: representative plots; right: statistical graphs). (F) Cell viability of NPC cells co-cultured with conditioned medium (CM) from differently treated macrophages, assessed by CCK-8 assay. (G) EdU staining (top) and quantification (bottom) to assess NPC cell proliferation. (H, I) Transwell assay evaluating the migration (H) and invasion (I) abilities of NPC cells (left: representative images, scale bar = 100 μm; right: quantification). Data are presented as mean ± SD; *P < 0.05, **P < 0.01, ***P < 0.001 (Student's t-test or one-way ANOVA). The original blotting images are shown in Supplementary Figure 2. The grouping of these blotting images is indicated by the white lines/ intervals between the lanes.

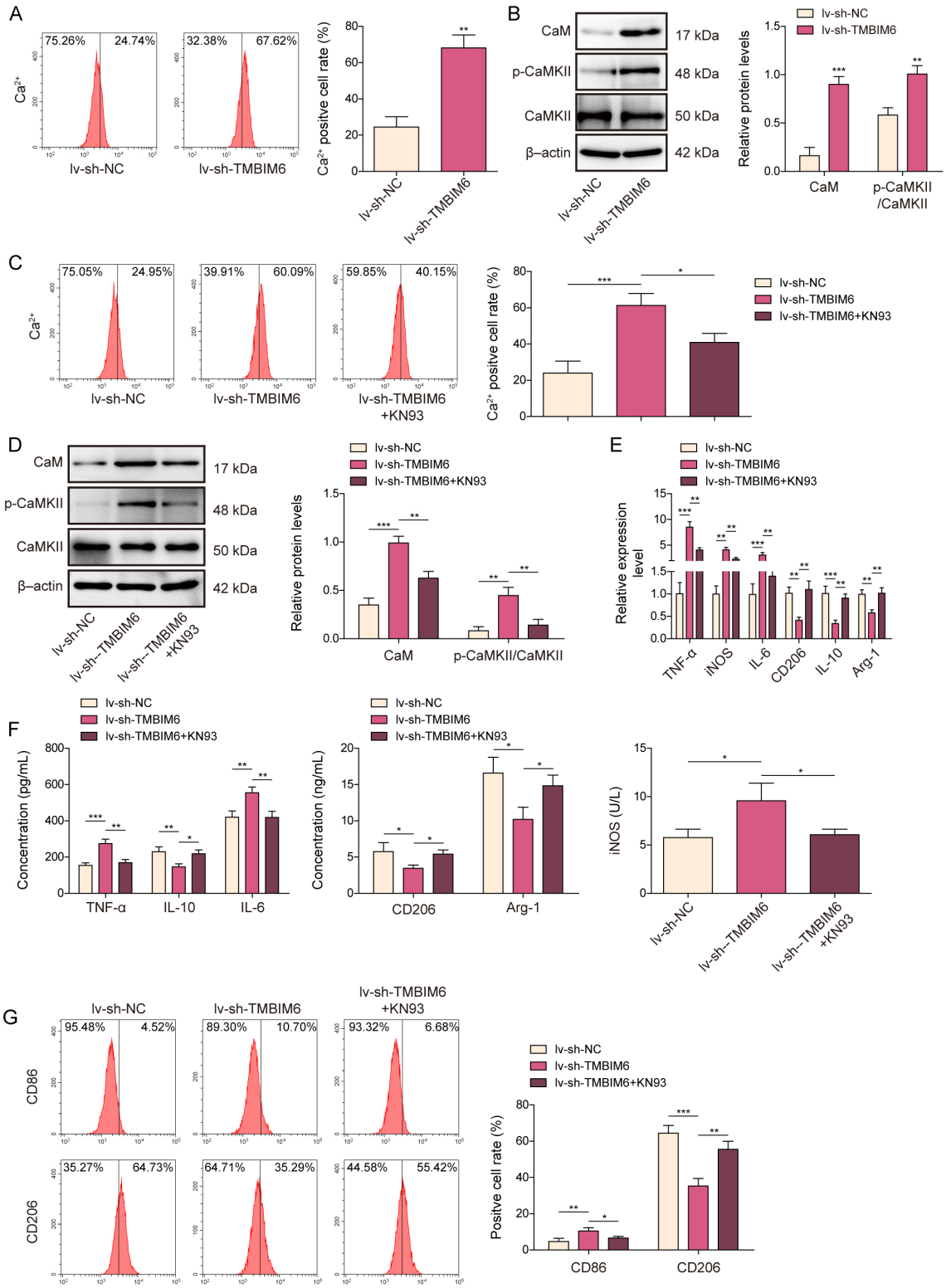

Figure 3

TMBIM6 regulates macrophage polarization via the Ca²⁺/CaM/CaMKII pathway.

(A) Flow cytometry (Fluo-4 AM staining) detection of intracellular Ca²⁺ concentration in M2 macrophages after TMBIM6 knockdown. (B) Western Blot (left) and quantification (right) of CaM and p-CaMKII protein expression after TMBIM6 knockdown. (C, D) Changes in intracellular Ca²⁺ concentration (C) and CaM/p-

CaMKII protein expression (D) after treatment with the CaMKII inhibitor KN93. (E, F) qRT-PCR (E) and ELISA (F) analysis of the reversal effects of KN93 on polarization marker expression. (G) Flow cytometry analysis of the regulatory effect of KN93 on CD86 and CD206 expression. Data are presented as mean ± SD; *P < 0.05, **P < 0.01, ***P < 0.001 (one-way ANOVA). The original blotting images are shown in Supplementary Figure 3. The grouping of these blotting images is indicated by the white lines/ intervals between the lanes.

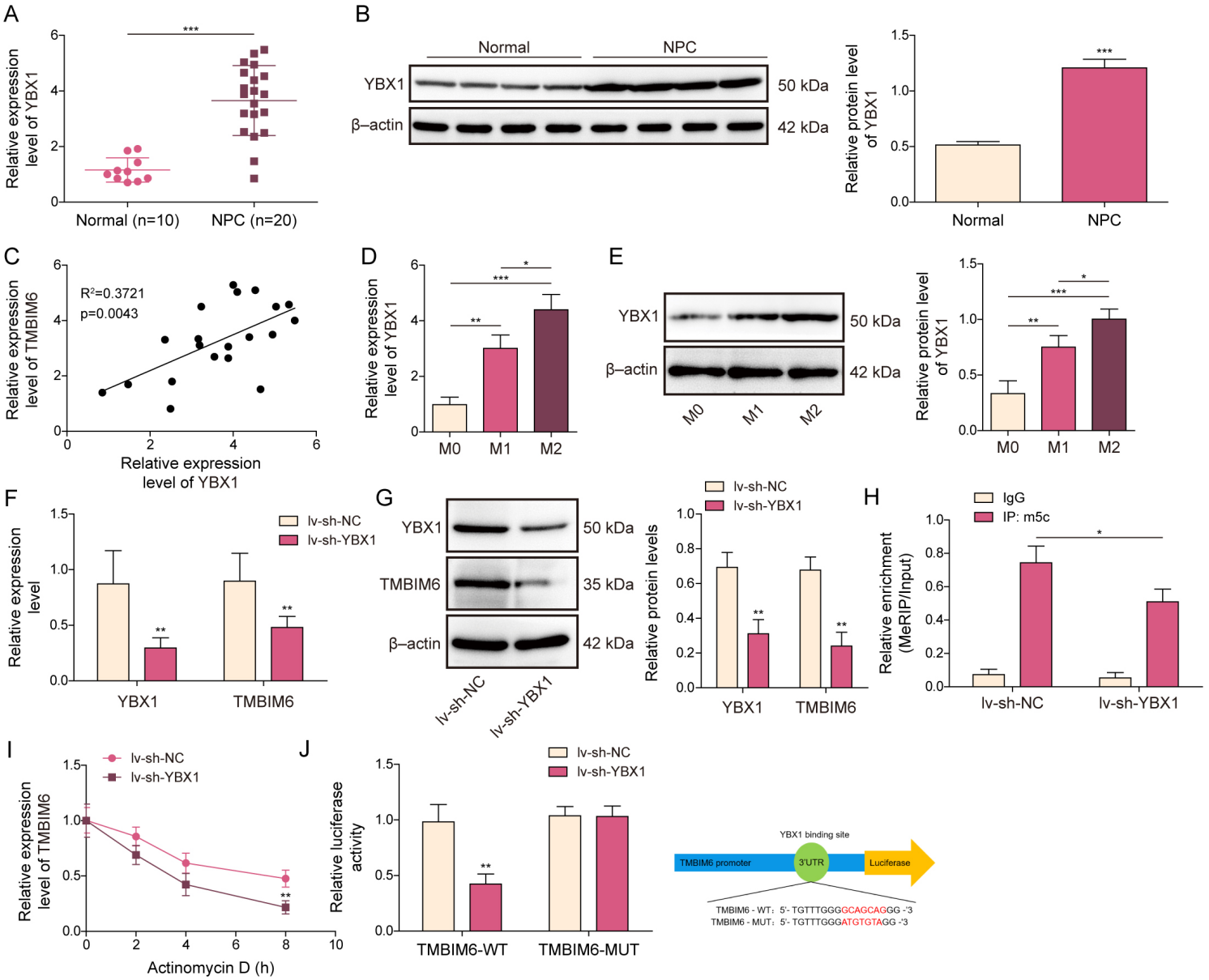

Figure 4

YBX1 stabilizes TMBIM6 mRNA and positively regulates its expression via m5C modification.

(A, B) qRT-PCR (A) and Western Blot (B) analysis of YBX1 expression in NPC and normal tissues. (C) Pearson correlation analysis between YBX1 and TMBIM6 protein expression levels. (D, E) qRT-PCR (D) and Western Blot (E) analysis of YBX1 expression in differently polarized macrophages. (F, G) qRT-PCR (F) and Western Blot (G) analysis of the effect of YBX1 knockdown on TMBIM6 expression. (H) MeRIP-

qPCR analysis of the effect of YBX1 knockdown on the m5C modification level of TMBIM6 mRNA. (I) Analysis of TMBIM6 mRNA stability after Actinomycin D (ActD) treatment. (J) Dual-luciferase reporter assay validating the regulation of wild-type (WT) or mutant (MUT) TMBIM6 3'UTR by YBX1. Data are presented as mean ± SD; *P < 0.05, **P < 0.01, ***P < 0.001. The original blotting images are shown in Supplementary Figure 4. The grouping of these blotting images is indicated by the white lines/ intervals between the lanes.

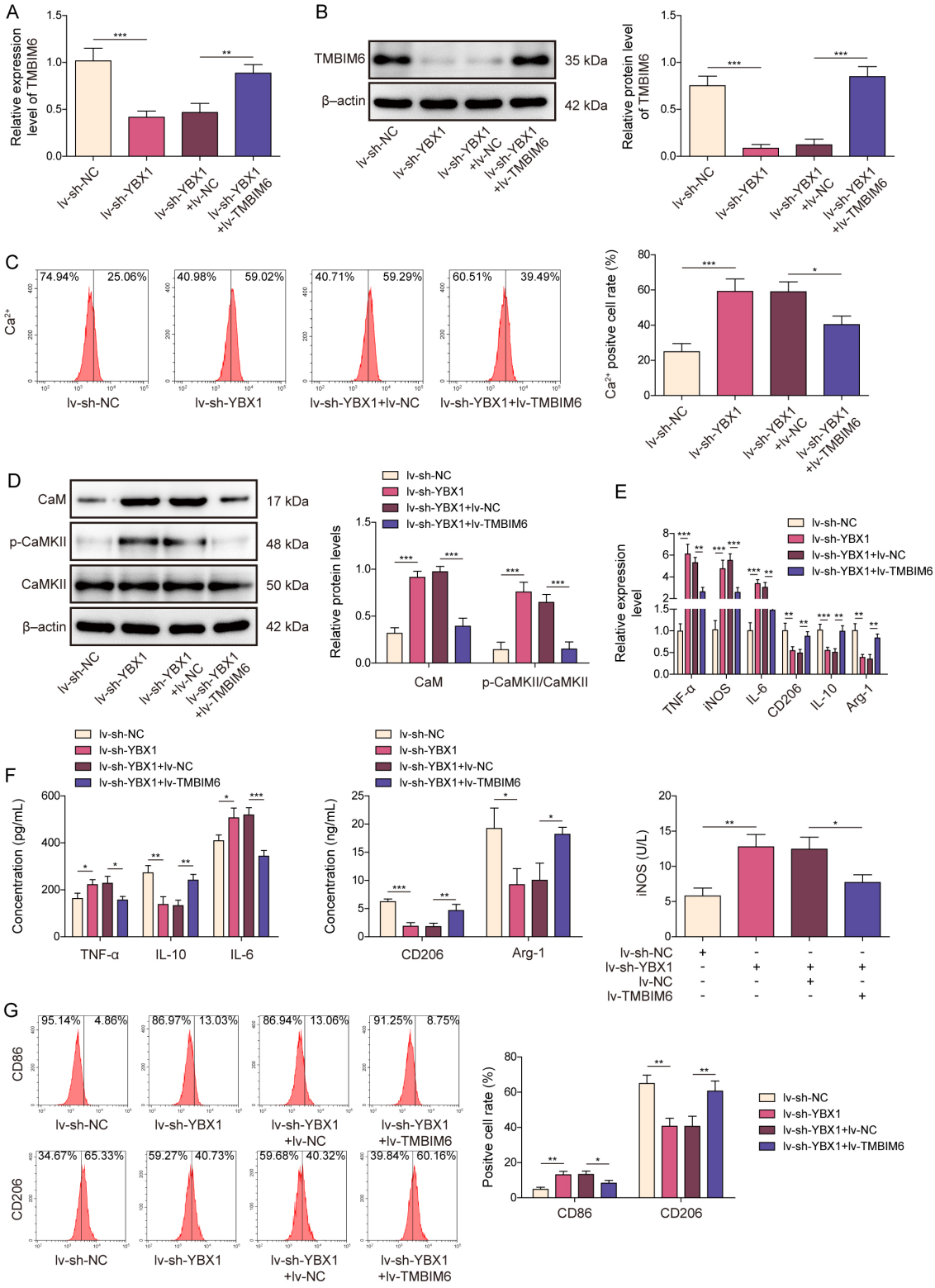

Figure 5

YBX1 influences macrophage polarization by regulating TMBIM6.

(A, B) qRT-PCR (A) and Western Blot (B) verification of TMBIM6 overexpression efficiency in the context of YBX1 knockdown. (C, D) Flow cytometry (C) and Western Blot (D) analysis of changes in Ca^{2+} levels and CaM/p-CaMKII protein expression in the rescue experiment. (E, F) qRT-PCR (E) and ELISA (F) analysis of changes in M1/M2 polarization marker expression in the rescue experiment. (G) Flow cytometry analysis of changes in CD86/CD206 surface expression in the rescue experiment. Data are presented as mean ± SD; *P < 0.05, **P < 0.01, ***P < 0.001 (one-way ANOVA). The original blotting images are shown in Supplementary Figure 5. The grouping of these blotting images is indicated by the white lines/ intervals between the lanes.

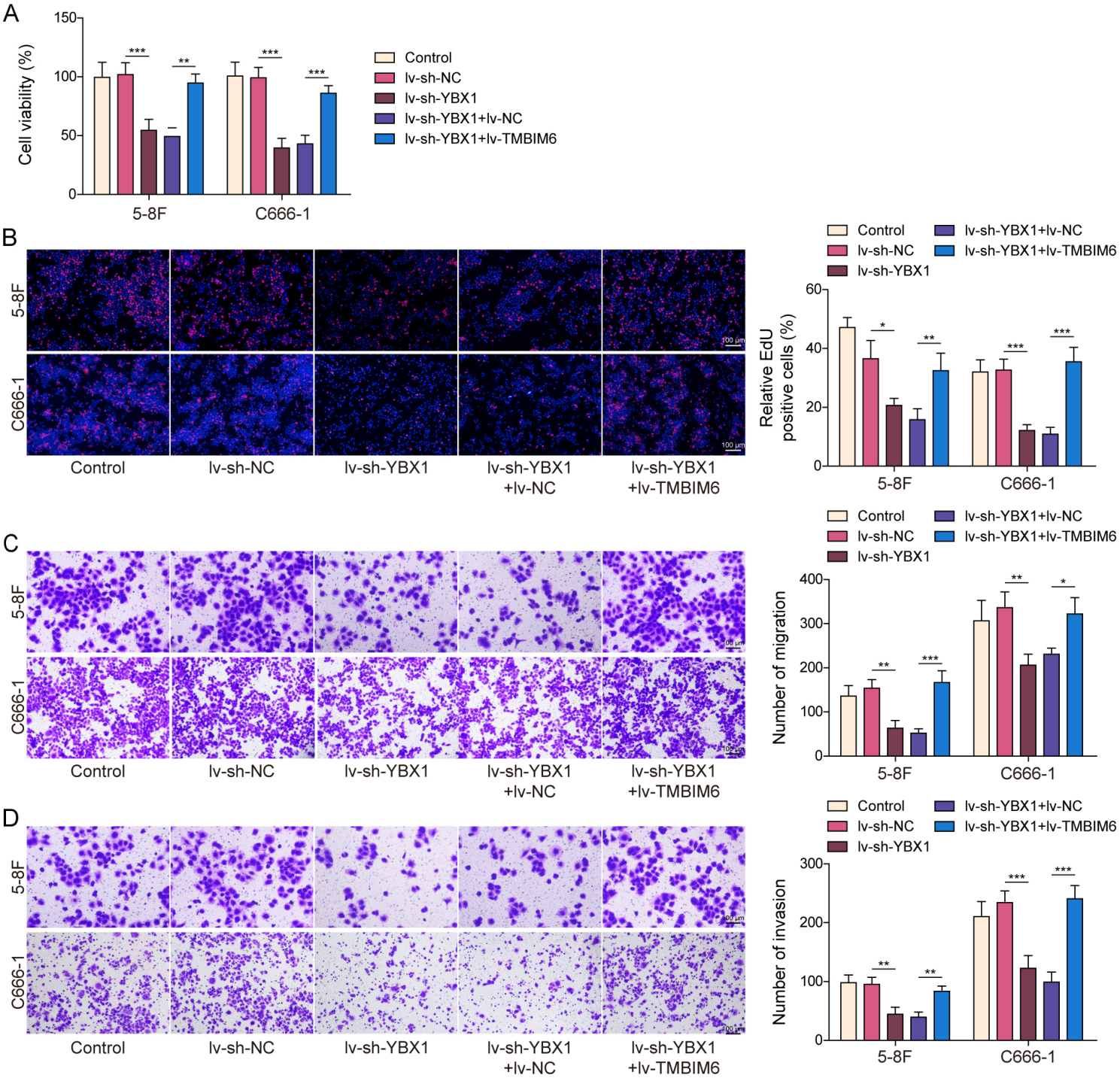

Figure 6

Knockdown of YBX1 inhibits the malignant phenotype of NPC cells by downregulating TMBIM6.

(A, B) CCK-8 (A) and EdU (B) assays evaluating the effects of YBX1 knockdown and TMBIM6 restoration on NPC cell viability and proliferation. (C, D) Transwell assays evaluating the effects of YBX1 knockdown and TMBIM6 restoration on NPC cell migration (C) and invasion (D) abilities. Data are presented as mean ± SD; *P < 0.05, **P < 0.01, ***P < 0.001 (one-way ANOVA).

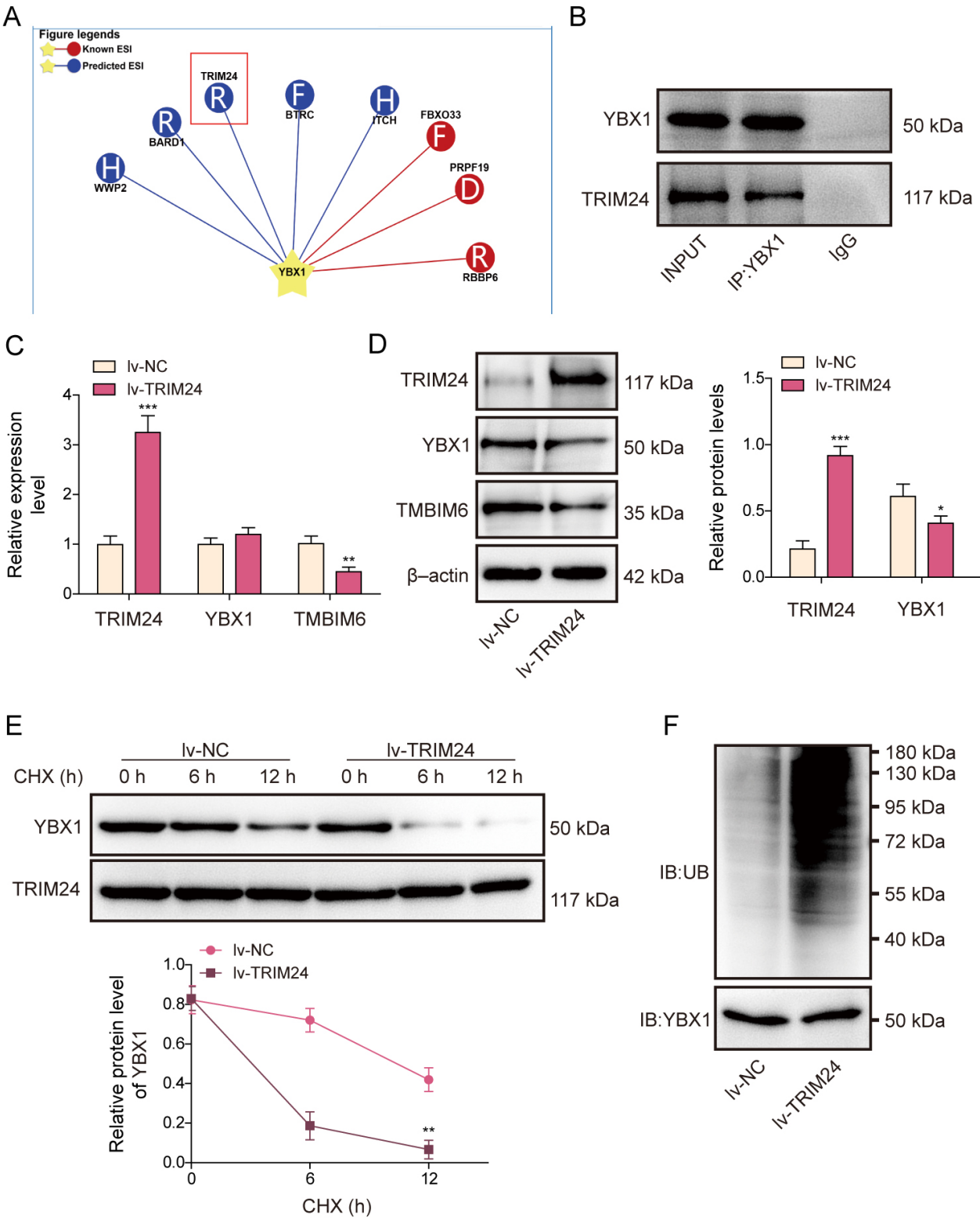

Figure 7

TRIM24 ubiquitinates and degrades YBX1.

(A) Ubibrowser database prediction of an interaction between TRIM24 and YBX1. (B) Co-IP experiment validating the intracellular interaction between TRIM24 and YBX1. (C, D) qRT-PCR (C) and Western Blot (D) analysis of the effects of TRIM24 overexpression on YBX1 and TMBIM6 expression. (E) Cycloheximide (CHX) chase assay analyzing the effect of TRIM24 overexpression on YBX1 protein stability. (F) Ubiquitination assay showing that TRIM24 overexpression promotes the polyubiquitination of YBX1. Data are presented as mean ± SD; *P < 0.05, **P < 0.01, ***P < 0.001. IB: immunoblot; IP: immunoprecipitation. The original blotting images are shown in Supplementary Figure 6. The grouping of these blotting images is indicated by the white lines/ intervals between the lanes.

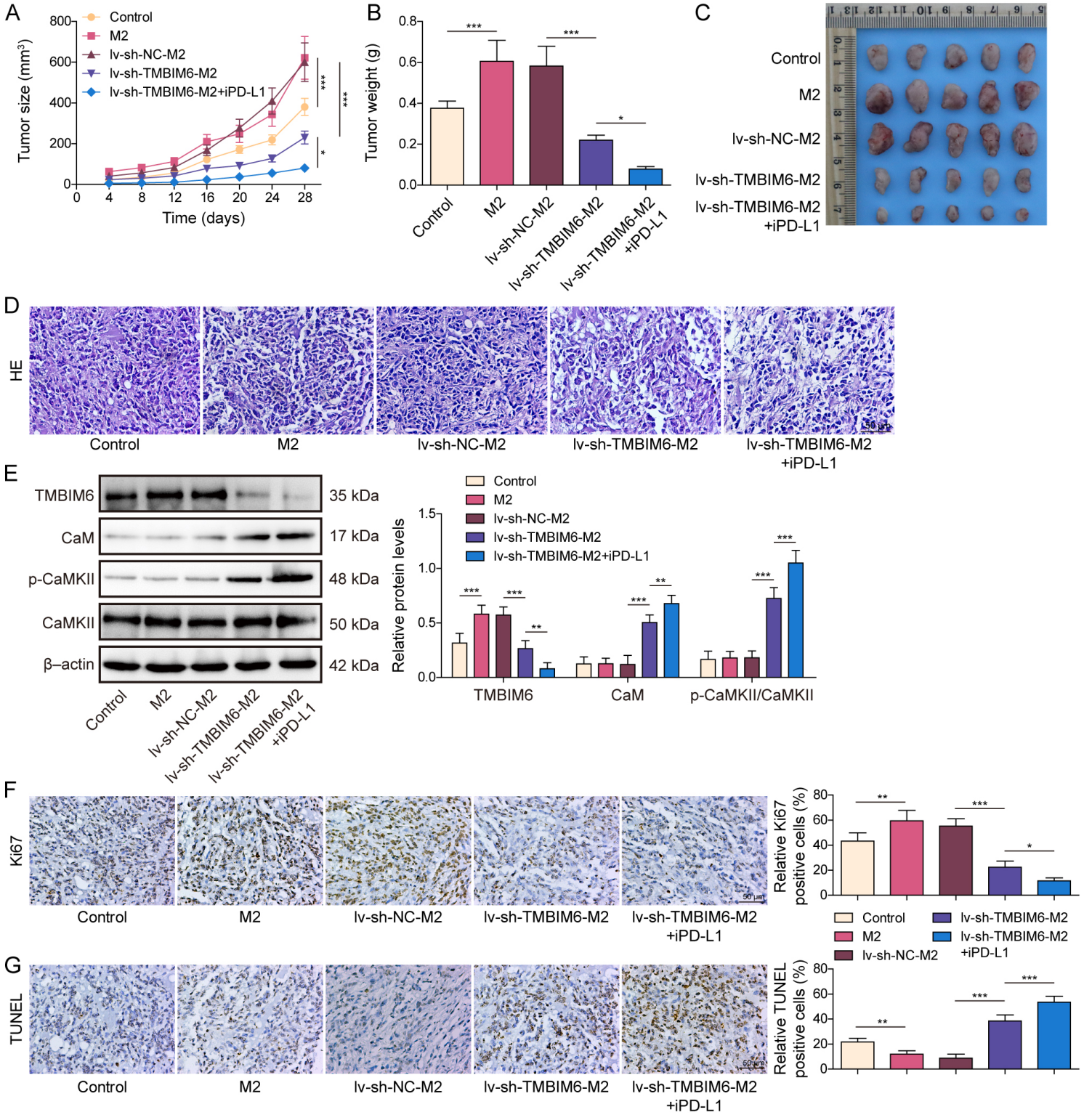

Figure 8

Targeting the TMBIM6 axis synergizes with PD-L1 inhibitor to suppress NPC growth in vivo.

(A) Growth curves of subcutaneous xenograft tumors in nude mice. (B, C) Representative photographs of excised tumors (B) and statistical analysis of tumor weight (C) at the experimental endpoint. (D) H&E staining of tumor tissues (scale bar = 50 μm). (E) Western Blot analysis of TMBIM6, CaM, and p-CaMKII protein expression in tumor tissue lysates. (F) Ki67 immunohistochemical staining (top) and

quantification of positive rate (bottom) (scale bar = 50 μm). (G) TUNEL apoptosis detection (top) and quantification of positive rate (bottom) (scale bar = 50 μm). Data are presented as mean ± SD (n = 4 mice per group); *P < 0.05, **P < 0.01, ***P < 0.001 (one-way ANOVA). The original blotting images are shown in Supplementary Figure 7. The grouping of these blotting images is indicated by the white lines/ intervals between the lanes.

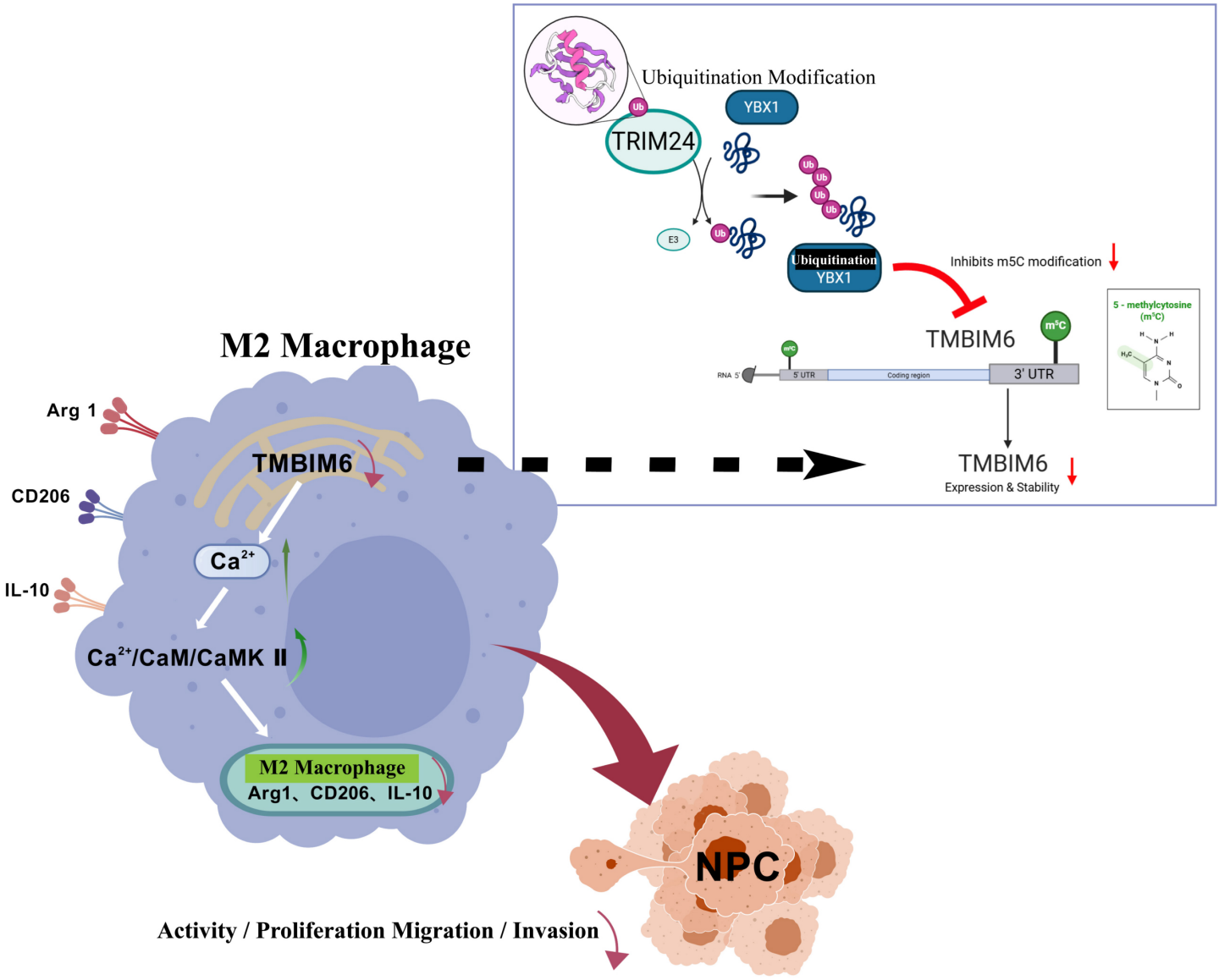

Figure 9

Schematic model summarizing the TRIM24/YBX1/TMBIM6/Ca^{2+} axis regulating M2 macrophage polarization in NPC.

Supplementary Files

This is a list of supplementary files associated with this preprint. Click to download.

- SupplementaryTable.docx
- SupplementaryInformationWesternBlotOriginalImages.pdf
- TheproteinconcentrationintheWesternblotexperiment.xlsx
- GrayscaleanalysisofWesternblotexperiment.xlsx